PALEONTOLOGY

Human footprints provide snapshot of last interglacial ecology in the Arabian interior

Mathew Stewart[1,2,3]*, Richard Clark-Wilson[4]*, Paul S. Breeze[5], Klint Janulis[6†], Ian Candy[4], Simon J. Armitage[4,7], David B. Ryves[8], Julien Louys[9], Mathieu Duval[9,10], Gilbert J. Price[11], Patrick Cuthbertson[12], Marco A. Bernal[13], Nick A. Drake[5,2], Abdullah M. Alsharekh[14], Badr Zahrani[15], Abdulaziz Al-Omari[15], Patrick Roberts[2], Huw S. Groucutt[1,2,3], Michael D. Petraglia[2,16,17]*

The nature of human dispersals out of Africa has remained elusive because of the poor resolution of paleoecological data in direct association with remains of the earliest non-African people. Here, we report hominin and non-hominin mammalian tracks from an ancient lake deposit in the Arabian Peninsula, dated within the last interglacial. The findings, it is argued, likely represent the oldest securely dated evidence for *Homo sapiens* in Arabia. The paleoecological evidence indicates a well-watered semi-arid grassland setting during human movements into the Nefud Desert of Saudi Arabia. We conclude that visitation to the lake was transient, likely serving as a place to drink and to forage, and that late Pleistocene human and mammalian migrations and landscape use patterns in Arabia were inexorably linked.

INTRODUCTION

Southwest Asia represents the main biogeographical gateway between Africa and Eurasia (*1*) and is, therefore, key for understanding hominin and faunal dispersal and evolution across continents. Fossils of *Homo sapiens* are first recorded outside of Africa ~210 and ~180 thousand years (ka) ago in southern Greece (*2*) and the Levant (*3*), respectively, and recent fossil evidence demonstrates the arrival of our species in the Arabian interior by at least ~85 ka (*4*). Understanding the nature of early *H. sapiens* out-of-Africa dispersals, however, has remained challenging owing to the poor resolution of paleoenvironmental and paleoecological data in direct association with remains of the earliest non-African people (*5*).

Here, we report hominin and non-hominin mammal footprints and fossils from the Alathar lacustrine deposit in the western Nefud Desert, Saudi Arabia (Fig. 1). We argue that the footprints, dated to the last interglacial and therefore contemporaneous with an early *H. sapiens* out-of-Africa dispersal (Fig. 2) (*6*), most likely represent the earliest evidence of our species in the Arabian Peninsula. The unique setting and taphonomic factors affecting the long-term preservation of footprints mean that groups of footprints, and particularly those in similar states of preservation, can be assumed to have been generated within a very short window, typically within a few hours or days (see full discussion in text S5) (*7*–*9*). An experimental study of modern human footprints in mud flats found that fine details were lost within 2 days and prints were rendered unrecognizable within four (*7*), and similar observations have been made for other non-hominin mammal tracks (*9*). The findings presented here, therefore, provide a unique opportunity to examine the close ecological interplay between late Pleistocene humans, animals, and their environments as our species began to venture into Eurasia.

RESULTS AND DISCUSSION

Geology and geochronology

The Alathar paleolake deposit lies as an inverted relief feature within an interdunal depression in the south-western portion of the Nefud Desert sand sea (Fig. 1). The sedimentary sequence comprises a ~1.8-m-thick deposit of sandy-silt diatomite (units 2 to 7) underlain by wind-blown sands (unit 1) (Fig. 3 and text S1). Two paleolake sections were recorded at the site and a composite section formed from both (Fig. 3). The first section (units 2 to 4) is exposed along the south-western margin of the deposit, and the footprints were found in the uppermost portion of unit 4b (i.e., the surface). A small number of fossils ($n = 4$) were also found eroding out of the surface of this unit. The second section (units 5 to 7) is located along parts of the western edge and toward the center of the modern-day surface of the paleolake deposit and stratigraphically overlies the footprint-bearing unit. The stratigraphic relationship between the two sections was visually correlated in the field based on lithostratigraphy. Samples for optically stimulated luminescence (OSL) dating were taken from sediments directly below (unit 2; PD61) and above (unit 5; PD62) the footprint-bearing unit and yielded ages of 121 ± 11 and 112 ± 10 ka, respectively, effectively bracketing the age

[1]Extreme Events Research Group, Max Planck Institute for Chemical Ecology, Hans-Knöll-Strasse 8, 07745 Jena, Germany. [2]Department of Archaeology, Max Planck Institute for the Science of Human History, Kahlaische Strasse 10, D-07743 Jena, Germany. [3]Max Planck Institute for Biogeochemistry, Hans-Knöll-Strasse 10, 07745 Jena, Germany. [4]Department of Geography, Royal Holloway, University of London, London, Egham, Surrey TW20 0EX, UK. [5]Department of Geography, King's College London, London, UK. [6]School of Archaeology, University of Oxford, 36 Beaumont Street, Oxford OX1 2PG, UK. [7]SFF Centre for Early Sapiens Behaviour (SapiensCE), University of Bergen, Post Box 7805, 5020 Bergen, Norway. [8]Geography and Environment, Loughborough University, Loughborough, Leics LE11 3TU, UK. [9]Australian Research Centre for Human Evolution (ARCHE), Environmental Futures Research Institute, Griffith University, Nathan, QLD, Australia. [10]Centro Nacional de Investigación sobre la Evolución Humana (CENIEH), Burgos09002, Spain. [11]School of Earth and Environmental Sciences, University of Queensland, St. Lucia QLD 4072, Australia. [12]Department of Early Prehistory and Quaternary Ecology, University of Tübingen, Tübingen, Germany. [13]Fundación Instituto de Investigación de Prehistoria y Evolución Humama. PALEOMÁGINA, Centro de Investigaciones Prehistóricas de Sierra Mágina Calle Nueva s/n; 23537 Bedmar (Jaén), Spain. [14]Department of Archaeology, College of Tourism and Archaeology, King Saud University, Riyadh, Saudi Arabia. [15]Saudi Commission for Tourism and National Heritage, Riyadh, Saudi Arabia. [16]Human Origins Program, National Museum of Natural History, Smithsonian Institution, Washington, DC 20013, USA. [17]School of Social Science, University of Queensland, St. Lucia, QLD 4072, Australia.
*Corresponding author. Email: mstewart@ice.mpg.de (M.S.); richard.clark-wilson@rhul.ac.uk (R.C.-W.); petraglia@shh.mpg.de (M.D.P.)
†Present address: Center for Cognitive Archeology, University of Colorado Colorado Springs, Colorado Springs, CO 80918, USA.

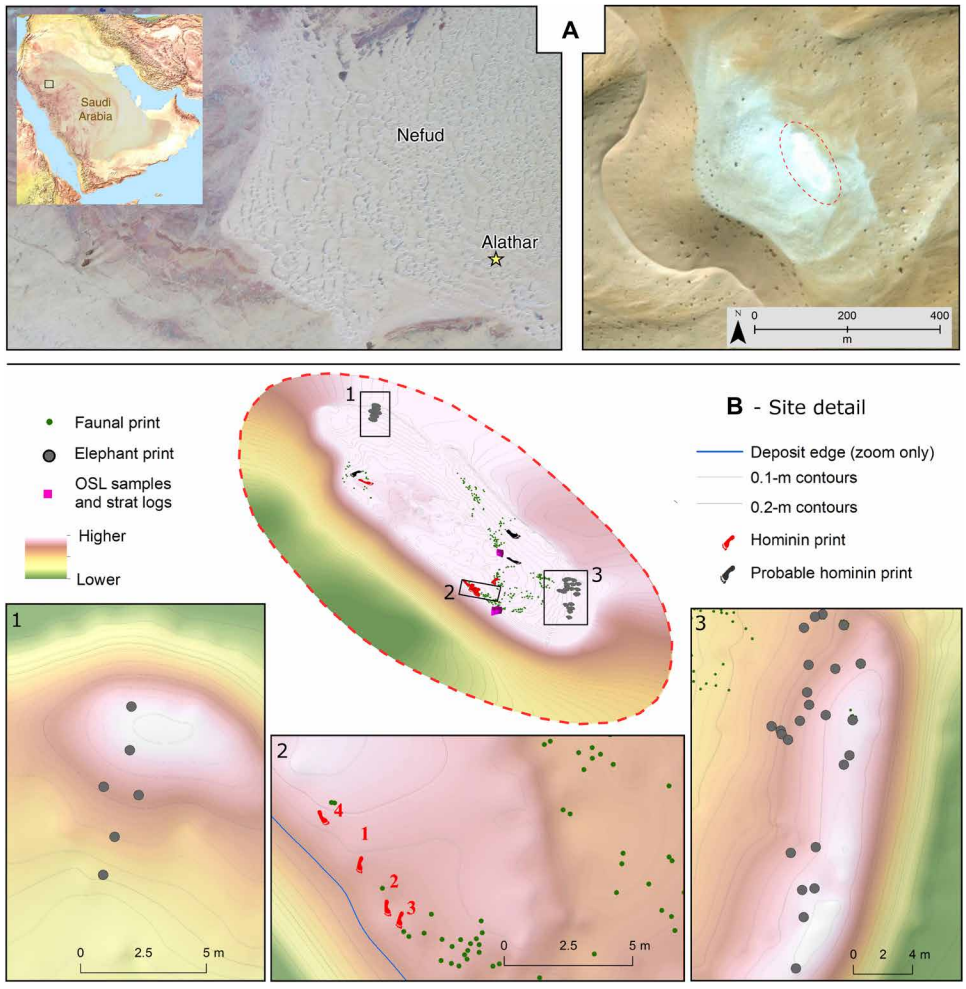

Fig. 1. The location of the Alathar paleolake site. (**A**) Map showing the location of the site within the western Nefud Desert, Saudi Arabia. (**B**) Three-dimensional oblique map of the site and location of tracks, fossils, and optically stimulated luminescence (OSL) samples.

of the prints (Fig. 3 and text S2). Diatom paleoecology and sedimentary analysis indicate that Alathar was an oligotrophic (nutrient-poor) and shallow freshwater lake for the majority of its existence (text S1). This is consistent with similar-aged nearby freshwater paleolake deposits (*4*, *10*–*11*) situated in the southern reaches of a "freshwater corridor" that connected the Arabian interior to the Levant and northeast Africa at times during marine isotope stage 5 (MIS 5; ~130 to 80 ka) (*12*). The presence of freshwater lakes in the western Nefud Desert provided a vital resource and habitable landscape for hominins and animals.

Fossil and footprint evidence

The freshwater lake at Alathar attracted a variety of large mammals, as represented by hominin, elephant, equid, and bovid tracks and fossils (Figs. 4 and 5, and text S5). The lake surface is heavily trampled, which probably reflects a dry season during which herbivores congregate around diminishing water supplies (*13*–*14*), and is consistent with sedimentary evidence for the drying up of the lake at that time (text S1). A total of 376 footprints were recorded, of which 177 could be either confidently or provisionally referred to an ichnotaxon. Seven hominin footprints were confidently identified, and given the fossil and archeological evidence for the spread of *H. sapiens* into the Levant and Arabia during MIS 5 (*4*, *6*, *15*–*19*) and absence of *Homo neanderthalensis* from the Levant at that time (*20*), we argue that *H. sapiens* was responsible for the tracks at Alathar (text S5). In addition, the size of the Alathar footprints is more consistent with those of early *H. sapiens* than *H. neanderthalensis* (fig. S9 and text S5).

Four of the human prints (HPR001 to HPR004) were found adjacent to one another along the south-western edge of the paleolake exposure (Figs. 1 and 4). Given their similar orientation, distances from one another, and differences in size, they are interpreted as two, or up to three, individuals traveling in concert. Although the human track sample is small, three important observations can be made from the trace and body fossils preserved at the site. First, the tracks are scattered across the paleolake and orientated in various directions, indicating that they were not simply traversing the lake but were engaged in nondirectional activities. Second, the human tracks, similar to many of the animal tracks, indicate movement in a mostly southward direction. Last, the body fossils recovered show no evidence for butchery, nor were any stone tools recovered at the site, although the former may be due to the poor surface preservation of

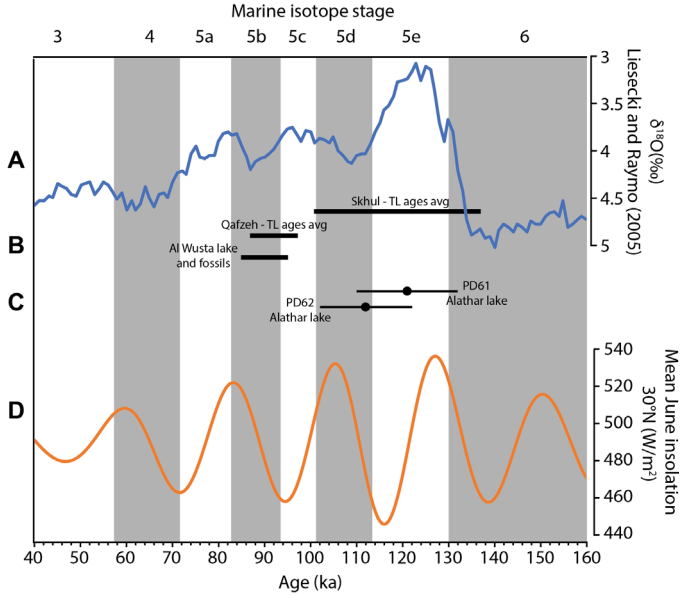

Fig. 2. Critical dates relating to fossil evidence for *H. sapiens* outside of Africa during MIS 5 compared with the bracketed age for the Alathar footprints. (**A**) LR04 stack (top) (blue line) displaying the marine $\delta^{18}O$ record (*62*). (**B**) Dated evidence for *H. sapiens* occupation of the Levant and the western Nefud Desert based on fossil evidence. Ages for occupation of the Levant are based on thermoluminescence (TL) ages from Skhul (*63*) and Qafzeh (*64*); see (*65*) for more detailed discussion. Al Wusta lake and fossils represent the Bayesian modeled age for units 2 and 3 (carbonate lake sediment and waterlain sands) (*4*). (**C**) OSL ages for the two lake samples from Alathar between which the hominin and faunal footprints lie (this study). (**D**) Summer insolation at 30°N (bottom) (orange line) (*66*).

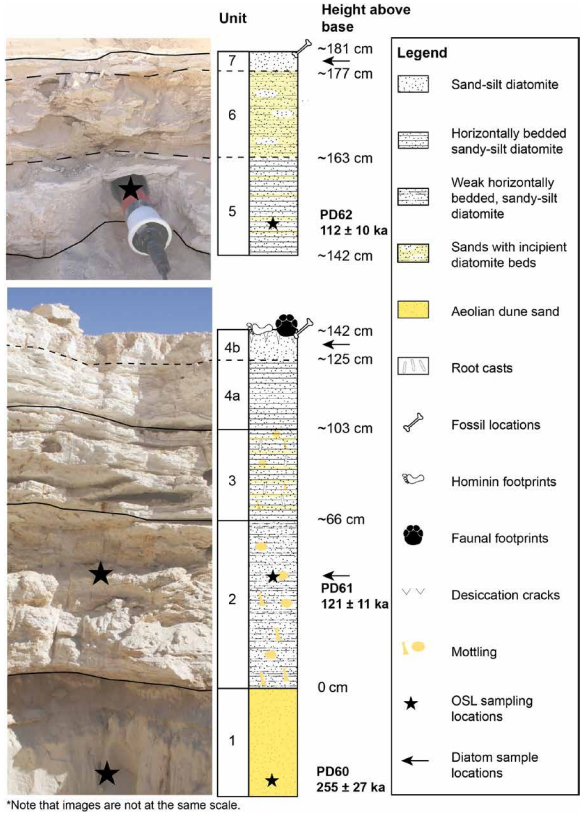

Fig. 3. Full sedimentary sequence from Alathar with location of OSL dates shown by stars. The first section (bottom) (units 1 to 4b) lies stratigraphically below the second section (top) (units 5 to 7). The two sections were located ~30-m apart (see "OSL samples and strat logs" in Fig. 1), and the stratigraphic relationship between them is easily traced in the field. All footprints are located on the top of the first section (unit 4b) but beneath the second section. Photo credit: Richard Clark-Wilson, Royal Holloway, University of London.

the fossils (text S5). This contrasts with other paleolake deposits in the western Nefud Desert that document intensive and repeated use of lake margin habitats by late Pleistocene hominins (*16*, *19*, *21*). From these observations, it appears that the Alathar lake was only briefly visited by humans. It may have served as a stopping point and place to drink and forage during long-distance travel, perhaps initiated by the arrival of dry conditions and dwindling water resources.

Elephant ($n = 43$) and camel ($n = 107$) footprints are most abundant and document herds (i.e., adults and juveniles) moving through the landscape (Fig. 5). Animal tracks are overall randomly orientated (Rayleigh's $R = 0.142$, $P < 0.393$), suggesting that movement in the vicinity of the lake was not geographically or geologically constrained, probably reflecting an open landscape (fig. S9). Some tracks clearly document individuals traveling to and from the lakeshore, which was situated southwest of the present-day exposure (text S1). Nevertheless, an overarching north-south trend is perhaps more consistent with movements tied to seasonal shifts in rainfall as opposed to water resource acquisition, as the latter typically involves movements perpendicular to the lakeshore among herbivores (*7*). This is particularly evident in the elephant tracks that are disproportionately orientated southward (Rayleigh's $R = 0.369$, $P < 0.001$), and similar north-south seasonal movements following lakes have been observed among modern elephant populations in East Africa (*22*). Elephants, in particular, suggest the regional presence of freshwater sources and substantial plant biomass (*23*), while the size of the tracks is suggestive of a species larger than any extant taxon (text S5). Elephants are notably absent from the nearby Levant from ~400 ka onward and considering their importance in the diets of Pleistocene hominins (*24*), their presence in Arabia may have made the region particularly attractive to dispersing *H. sapiens*. Some of the ungulate prints are consistent in shape and size with a giant buffalo, possibly *Syncerus*, a taxon previously identified at nearby MIS 5 sites (*4*, *25*). A single small equid track may represent wild ass, which were common in southwest Asia during the late Pleistocene (*26*), while a pair of ungulate prints are probably those of a medium-sized bovid (text S5).

In addition to footprints, 233 fossils were recovered and included remains of *Oryx* and elephant (text S5). The discovery of fossils eroding out of the footprint-bearing sediments and similar taxonomic representation across the footprints and fossils imply coeval formation of footprints and deposition of bones. However, direct U-series analysis of several fossil teeth seems to draw an unexpectedly more complex taphonomical history for some specimens of the fossil assemblage (see full discussion in text S4). Carnivores are inferred from tooth-marked bone, and it is likely that they were drawn to Alathar by the dense congregation of herbivores, as is observed in modern-day African savanna ecosystems (*27*). Stable carbon isotope ($\delta^{13}C$) analysis of fossil tooth enamel indicates substantial portions of C_4 grasses in the diets of herbivores, but with fewer lush grasses than in those from the nearby middle Pleistocene site of Ti's al Ghadah (fig. S11 and text S6) (*28*). Sequential isotope analysis of

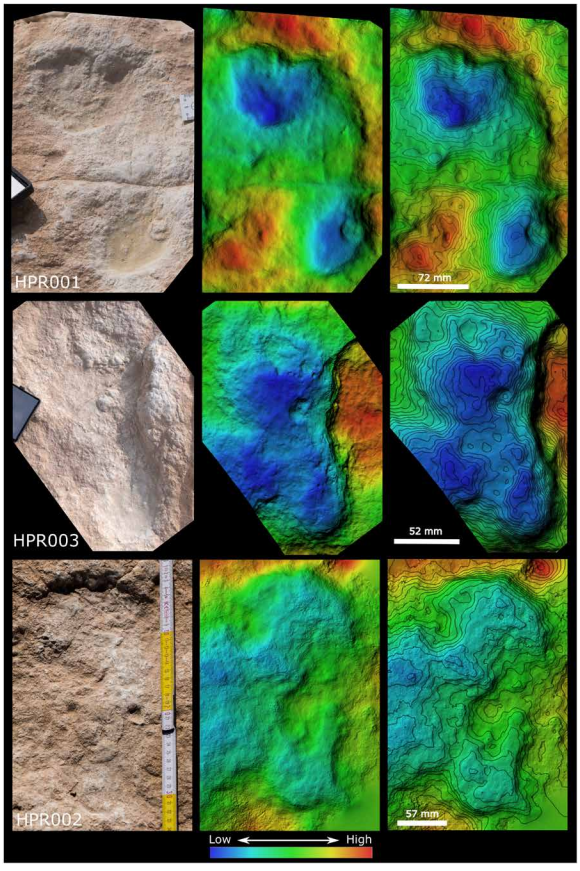

Fig. 4. Digital elevation models of three selected hominin tracks (HPR001, HPR002, and HPR003). Photo credit: Klint Janulis, University of Oxford.

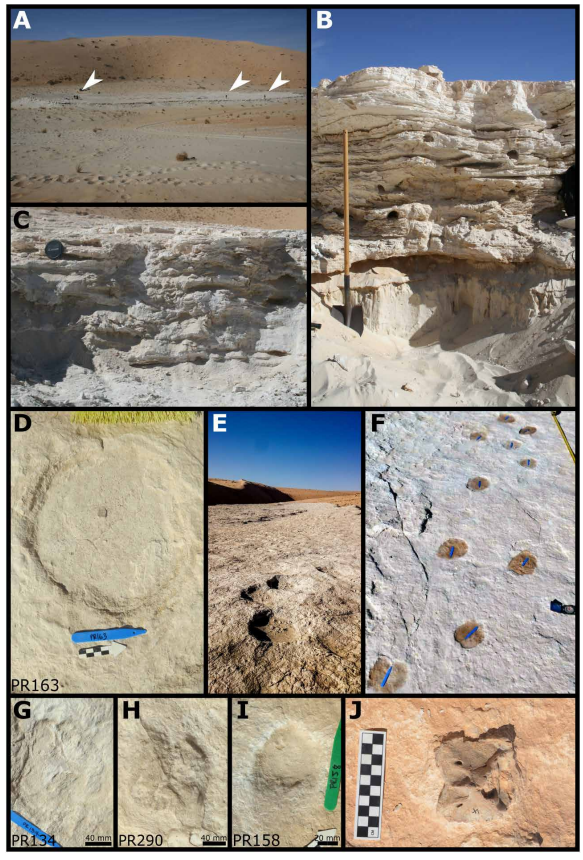

Fig. 5. The Alathar paleolake sediments, footprints, and fossils. (**A**) Plan view of the Alathar paleolake deposits with researchers indicated by white arrowheads. (**B**) First stratigraphic section (units FS1 to FS3). (**C**) Second stratigraphic section (units SS1 to SS3) overlying the first but located toward the center of the paleolake. (**D** and **E**) Example of an elephant track and trackway, *Proboscipeda* isp. (**F**) Camelid trackway, *Lamaichnum* isp. (**G**) Camelid forefoot (**H**) Camelid hindfoot. (**I**) Equid track, *Hippipeda* isp. (**J**) Bovid axis vertebra eroding out of the paleolake sediment. Photo credit: Gilbert Price, The University of Queensland and Richard Clark-Wilson, Royal Holloway, University of London.

elephant tooth enamel (fig. S12 and text S6) indicates a persistent source of water and vegetation that may also be explained by seasonal migrations, and similar results are reported at Ti's al Ghadah (TAG) (*28*).

CONCLUSIONS

Together, the sedimentary and ichnofossil data are consistent with a well-watered semi-arid grassland setting during a dry period. Lakes and rivers serve as focal points on the landscape for large mammals. During dry seasons, when resources are scarce and herbivores congregate around small watering holes, they are also attractive for hunters and, more often, forages (*29*). They may also act as effective corridors during seasonal migrations (*7*, *30*), and archaeological data suggest that late Pleistocene *Homo* in Arabia was highly mobile, penetrating deeper into the Arabian interior than their middle Pleistocene predecessors (*19*, *21*). We demonstrate a direct spatial and temporal association between late Pleistocene humans and medium and large herbivores, indicating that movements and landscape use by humans and mammals in Arabia were inexorably linked. The lack of archaeological evidence suggests that the Alathar lake was only briefly visited by people. These findings indicate that transient lakeshore use by humans during a dry period of the last interglacial was likely primarily tied to the need for potable water.

MATERIALS AND METHODS

Sedimentology and diatom analysis

Macroscale sedimentology

The paleolake deposit was initially surveyed to identify the best exposed sedimentary sequence for analysis. Once sections were identified, they were logged and described from the base of the paleolake sediments upward to determine the sedimentary structure (bedding and units) and texture (sorting and grain size). Samples for laboratory analysis were collected by extracting coherent blocks from each section. In the laboratory, these blocks were subsampled, powdered, and analyzed using Bascomb calcimetry (*31*) and whole-rock x-ray diffraction (XRD). XRD work was carried out in the Department of Earth Sciences, Royal Holloway, on a Philips PW1830/3020 spectrometer with copper Kα x-rays. Mineral peaks were identified manually from the International Centre for Diffraction Data (ICDD) Powder Diffraction File database.

Micromophology

A total of 14 thin section slides across the sedimentary sequences (see fig. S2 for sample locations) were prepared from fresh sediment blocks subsampled from larger block samples collected in the field.

Thin section preparation followed standard methods devised in the Centre for Micromorphology at Royal Holloway University of London (*32*). Thin sections were analyzed using an Olympus BX-50 microscope with magnifications from ×20 to ×200. Photomicrographs were captured with a Pixera Penguin 600es camera. Microfacies were qualitatively analyzed.

Diatom analysis

Three diatom samples were taken at 40 cm (unit 2), 140 cm (unit 4b), and 175 cm (unit 7) above the base level. Samples were prepared as follows. Approximately 0.1 g of dried sediment were placed into a centrifuge tube, immersed in 5 ml of 30% H_2O_2, and stored at room temperature until all organic material was removed. Samples were rinsed four times with deionized water and subsequently centrifuged for 4 min at 1200 rpm. The diatom suspension was diluted to a suitable concentration and then settled onto coverslips. These were left to air dry in a dust-free environment before mounting with a high-contrast medium (Naphrax). At least 315 diatom valves were counted for each sample (mean, 321 valves) under oil immersion with phase contrast illumination at ×1000. Quantitative reconstructions were carried out using the program C2 (v1.7.7) (*33*) (available at www.staff.ncl.ac.uk/stephen.juggins/software/C2Home.htm).

Analog matching of fossil samples was performed within the combined African salinity dataset (n = 370) from the European Diatom Database (*34*), which includes modern samples from northern and eastern Africa (*35*). The closest analogs in all cases included both eastern and northern African samples (in agreement with the geographic location of the site), and hence, the combined African dataset was used for our diatom-conductivity reconstructions. Inferred conductivity (microsiemens per centimeter) was derived from fossil assemblages (percent data) using a weighted average transfer function with inverse deshrinking. The conductivity model performs well when internally validated by bootstrapping with 999 cycles (r^2_{boot} = 0.755, Root Mean Squared Error of Prediction $(RMSEP)_{boot}$ = 0.466 log units) and provides sample-specific errors on diatom-inferred conductivity that are significantly smaller (0.12 to 0.14 log conductivity units) than the overall predicted model errors (fig. S4).

OSL dating

Sample collection, preparation, and analysis

Samples for luminescence dating were collected from the underlying dune sands and directly from the paleolake sediments. This sampling strategy yields direct ages for lake formation and humidity. Luminescence dating was carried out at the Royal Holloway Luminescence Laboratory, Royal Holloway University of London. All luminescence measurements presented here use the quartz OSL signal on 180 to 210-μm quartz grains, and measurements were carried out using a Risø TL/OSL-DA-15 automated dating system (*36*). Before single-aliquot measurement, purified quartz was placed as a 5-mm circular monolayer on a 9.7-mm-diameter stainless steel discs using Silkospray oil applied via a 5-mm mask. Equivalent doses were determined using the single-aliquot regenerative-dose protocol (*37*). The burial dose for each sample was calculated using the central age model (*38*). Environmental dose rates consisted of external beta, gamma, and cosmic ray components (table S3). Beta doses were calculated using a Risø GM-25-5 low-level beta counting system (*39*) with MgO and Volkagem loess standards (*40*) standards. Gamma dose rates were measured in the field using an EG&G ORTEC digi Dart-LF gamma spectrometer using the "threshold" method. Cosmic dose was calculated on the basis of location, altitude, and present day burial depth (*41*). A full description of the luminescence methods is provided in text S2.

Electron spin resonance and U-series dating

Samples and sample preparation

Five fossil teeth were selected for U-series and electron spin resonance (ESR) dating purposes (table S5 and fig. S7). All sampled specimens were recovered from the surface of the paleolake deposit and exhibit weathering and fragmentation characteristic of the assemblage (text S5). None of the teeth could be identified to the species level, but all can be attributed to bovid and at least two to *Oryx*. The teeth were prepared following the same standard ESR dating procedure based on enamel powder used earlier for the TAG fossil specimens (*42*): The enamel layer was mechanically separated from the other dental tissues, and both inner and outer surfaces were removed with a dentist drill to eliminate the volume that received an external alpha dose. The dentine attached to the enamel layer was kept aside for subsequent solution bulk U-series analyses. Enamel and dentine were ground and sieved <200 μm.

ESR dose evaluation

Dose evaluation used the multiple aliquot additive dose method. The enamel powder was split into 11 aliquots and irradiated with a Gammacell 1000 Cs-137 gamma source [dose rate, 6.4 grays (Gy)/min] to the following doses: 0.0, 80.1, 150.2, 250.5, 350.7, 500.8, 701.1, 901.6, 1502.6, 3005.2, and 5008.6 Gy. Room-temperature ESR measurements were carried out at the Centro Nacional de Investigación sobre la Evolución Humana (Burgos, Spain) with an EMXmicro 6/1 Bruker ESR spectrometer coupled to a standard rectangular ER 4102ST cavity. The following procedure was used to minimize the analytical uncertainties: (i) All aliquots of a given sample were carefully weighted into their corresponding tubes, and a variation of <1 mg was tolerated between aliquots; (ii) ESR measurements were performed using a Teflon sample tube holder inserted from the bottom of the cavity to ensure that the vertical position of the tubes remains exactly the same for all aliquots. The following acquisition parameters were used: 1 scan, 1-mW microwave power, 1024-point resolution, 15-mT sweep width, 100-kHz modulation frequency, 0.1-mT modulation amplitude, 20-ms conversion time, and 5-ms time constant. All aliquots of a given sample were measured within a short time interval (<1 hour). This procedure was repeated two to three times over successive days without removing the enamel from the ESR tubes between measurements to evaluate measurement and equivalent dose (D_E) precisions (table S6). The ESR intensities were extracted from T1-B2 peak-to-peak amplitudes of the ESR signal (*43*) and then normalized to the corresponding number of scans and aliquot mass. D_E values were obtained by fitting a single saturating exponential through the pooled ESR intensities derived from the repeated measurements. Fitting was performed with Microcal OriginPro 9.1 software, which is based on a Levenberg-Marquardt algorithm by chi-square minimization. Data were weighted by the inverse of the squared ESR intensity ($1/I^2$) (*44*). ESR dose-response curves are shown in fig. S8.

U-series analysis of dental tissues

Powdered enamel, dentine, and cement samples were weighed then spiked using a ^{229}Th-^{233}U tracer before being digested in concentrated HNO_3. The solutions were then treated with H_2O_2 to remove trace organics, with U and Th then separated using conventional column chemistry techniques described in (*45*). Both U and Th were collected into the same precleaned test tube using 3 ml of 2% HNO_3

mixed with a trace amount of hydrofluoric acid (HF). U-Th isotopic ratios were then measured using a Nu Plasma multicollector inductively coupled plasma mass spectrometer (MC-ICP-MS) in the Radiogenic Isotope Facility at The University of Queensland, Brisbane, Australia, following analytical protocols established by (*45*–*46*). Numerical results are given in table S7.

Dose rate and age calculations

No in situ evaluation of the gamma dose rate associated with the teeth was performed. Beta and gamma dose rates were derived from the laboratory analysis of two bulk sediment samples collected from the uppermost layer of the two sedimentary sections (Fig. 3): Ala-140 (0 to 6 cm below surface of unit 4b) and Ala-SCS (0 to 4 cm below surface of unit 7). MC-ICP-MS analyses were performed by Genalysis Laboratory Services, following a four-acid digest preparation procedure. The following results were obtained: U = 1.806 ± 0.004 ppm (parts per million), Th = 5.283 ± 0.021 ppm, and K = 0.686 ± 0.005% for Ala-140 and U = 0.649 ± 0.004 ppm, Th = 0.681 ± 0.003 ppm, and K = 1.098 ± 0.009% for Ala-SCS. Given the large variability observed between the two samples, initial dose rate calculations were performed using Ala-140 sediment sample, which best related to teeth #2 and #232 (fig. S7).

The following parameters were used for the dose rate calculations: an alpha efficiency of 0.13 ± 0.02 (*47*), Monte-Carlo beta attenuation factors from (*48*), dose-rate conversion factors from (*49*), an estimated water content of 5 ± 3 and 5 ± 2.5 weight % in dentine and sediment, respectively. These values were used to derive the beta and gamma dose rate components. The thickness of the overburden was assumed to be 0.5 ± 0.2 m. Cosmic dose rate was calculated using (*50*).

Age calculations were performed with USESR, a MATLAB-based program (*51*) using the Uranium series (US) model defined by (*52*). The accelerating uptake model (*53*) that can take into account uranium leaching was also tested. Additional closed system U-series (CSUS)–ESR age calculations were also carried out using DATA program (*54*). The closed system (CS) model defined by (*55*) is based on the assumption of a closed system behavior after a rapid uranium uptake event in dental tissues. The CSUS-ESR age is usually considered as providing a maximum age constraint for the fossil. US and CSUS models are typically considered to encompass all possible uptake scenarios.

Fossil and ichnofossil analysis

Fossil analysis

Fossils were systematically collected during pedestrian surveys across the site and their position recorded using a Differential Global Positioning System. Pedestrian surveys were conducted by three to five people walking together in a straight line and separated by not more than 2 m. The entire exposure of the paleolake was examined, and all fossils regardless of size were collected. Each fossil specimen was identified to the lowest taxonomic level possible and facilitated by osteological collections housed at the University of New South Wales, Australia and the Smithsonian National Museum of Natural History, USA. Each specimen was examined by eye and hand lens (10× to 20×), and bone surface modifications were identified and recorded following standard methodologies [e.g., (*56*–*57*)].

Footprint analysis

Footprints were systematically documented during pedestrian surveys across the site, and their position was recorded using a Leica Total Station. Each print was photographed with a scale, compass, and arrow denoting orientation of movement when discernible (e.g., Fig. 3I), and track length and width were recorded. Directionality was assessed using Rayleigh's Z test for uniformity for circular data and a Watsons U^2 test for von Mises normal distribution. Three hominin tracks (HPR001, HPR002, and HPR003) were extensively photographed to generate high-resolution, scaled three-dimensional models (AgiSoft PhotoScan Professional, Agisoft LLC, St. Petersburg, Russia). Additional total station points (~15 points for each) were taken to map the print outline, as well as high and low points in and around the prints, and these acted as ground control points during model generation. Print morphometric data were collected in the field following (fig. S9A) (*58*). Footprint index was calculated by dividing footprint length (FPL) (Heel-Hallux) by ball breadth (B1 and B2).

Hominin stature, body mass, and speed estimates were calculated following (*59*) and based on regression equations derived from footprint morphometric data of modern, habitually unshod Daasanach people (Lake Turkana region, Kenya), a group that inhabits a semi-arid grassland environment likely similar to the western Nefud Desert during the Pleistocene humid phases (*4*). Stature was determined from FPL, body mass from footprint area [FP area = FPL × ball width (BW)], and speed from stride length (SL; distance from the heel of one step to the heel of the next step made by the same foot) divided by average FPL (SL/avgFPL). Comparative stature and mass data for late Pleistocene *H. sapiens* (n = 89) and *H. neanderthalensis* (n = 51) were sourced from the literature and based on allometric relationships between limb bone size and body height (fig. S10). Values were averaged in instances where multiple estimates existed for a single individual (e.g., the Skhul IV hominin).

Stable isotope analysis

Eight samples, which comprise seven Bovidae teeth and one elephant tooth, were selected for stable carbon and oxygen isotope analysis of tooth enamel from the available fossil material recovered from atop modern-day paleolake deposit (table S14 and fig. S11). The elephant molar was used for additional, sequential stable carbon and oxygen analysis based on its completeness and robustness to endure additional sampling (table S15 and fig. S12). Fourier transform infrared spectroscopy was used to assess enamel preservation as per (*28*).

All teeth or teeth fragments were cleaned using air abrasion to remove any adhering external material. Enamel powder for bulk analysis was obtained using gentle abrasion with a diamond-tipped drill along the full length of the buccal surface to ensure a representative measurement for the entire period of enamel formation. For sequential samples, each sample was a 1- to 2-mm-wide groove perpendicular to the tooth growth axis, through the thickness of the enamel layer. The distance of the base of each sample groove from the enamel/root junction from the furthest sample margin was recorded. All enamel powder was pretreated to remove organic or secondary carbonate contaminates. This consisted of a series of washes in 1.5% sodium hypochlorite for 60 min, followed by three rinses in purified H_2O and centrifuging, before 0.1 M acetic acid was added for 10 min, followed by another three rinses in purified H_2O [as per (*60*–*61*)].

Following reaction with 100% phosphoric acid, gases evolved from the samples were analyzed to stable carbon and oxygen isotopic composition using a Thermo Gas Bench 2 connected to a Thermo Delta V Advantage mass spectrometer at the Department of Archaeology, Max Planck Institute for the Science of Human History. Carbon

and oxygen isotope values were compared against international standards (NBS 19, Merck) registered by the International Atomic Energy Agency. Replicate analysis of ostrich egg shell (OES) standards suggests that machine measurement error is *c.* ±0.1‰ for $\delta^{13}C$ and ±0.2‰ for $\delta^{18}O$. Overall measurement precision was studied through the measurement of repeat extracts from a bovid tooth enamel standard ($n = 40$, ±0.2‰ for $\delta^{13}C$ and ±0.3‰ for $\delta^{18}O$).

SUPPLEMENTARY MATERIALS

Supplementary material for this article is available at http://advances.sciencemag.org/cgi/content/full/6/38/eaba8940/DC1

REFERENCES AND NOTES

1. H. J. O'Regan, A. Turner, L. C. Bishop, S. Elton, A. L. Lambm, Hominins without fellow travellers? First appearances and inferred dispersals of Afro-Eurasian large-mammals in the Plio-Pleistocene. *Quat. Sci. Rev.* **30**, 1343–1352 (2011).
2. K. Harvati, C. Röding, A. M. Bosman, F. A. Karakostis, R. Grün, C. Stringer, P. Karkanas, N. C. Thompson, V. Koutoulidis, L. A. Moulopouls, V. G. Gorgoulis, M. Kouloukoussa, Apidima Cave fossils provide earliest evidence of *Homo sapiens* in Eurasia. *Nature* **571**, 500–504 (2019).
3. I. Hershkovitz, G. W. Weber, R. Quam, M. Duval, R. Grün, L. Kinsley, A. Ayalon, M. Bar-Matthews, H. Valladas, N. Mercier, J. L. Arsuaga, M. Martinón-Torres, J. M. Bermúdez, de Castro, C. Fornai, L. Martín-Francés, R. Sarig, H. May, V. A. Krenn, V. Slon, L. Rodríguez, R. García, C. Lorenzo, J. M. Carretero, A. Frumkin, R. Shahack-Gross, D. E. B.-Y. Mayer, Y. Cui, X. Wu, N. Peled, I. Groman-Yaroslavski, L. Weissbrod, R. Yeshurun, A. Tsatskin, Y. Zaidner, M. Weintein-Evron, The earliest modern humans outside Africa. *Science* **359**, 456–459 (2018).
4. H. S. Groucutt, R. Grün, I. S. Zalmout, N. A. Drake, S. J. Armitage, I. Candy, R. Clark-Wilson, J. Louys, P. S. Breeze, M. Duval, L. T. Buck, T. L. Kivell, E. Pomeroy, N. B. Stephens, J. T. Stock, M. Stewart, G. J. Price, L. Kinsley, W. W. Sung, A. Alsharekh, A. al-Omari, M. Zahir, A. M. Memesh, A. J. Abdulshakoor, A. M. Al-Masari, A. A. Bahameen, K. M. S. Al Murayyi, B. Zahrani, E. M. L. Scerri, M. D. Petraglia, *Homo sapiens* in Arabia by 85,000 years ago. *Nat. Ecol. Evol.* **2**, 800–809 (2018).
5. P. Roberts, B. A. Stewart, Defining the 'generalist specialist' niche for Pleistocene *Homo sapiens*. *Nat. Hum. Behav.* **2**, 542–550 (2018).
6. R. Grün, C. Stringer, F. McDermott, R. Nathan, N. Porat, S. Robertson, L. Taylor, G. Mortimer, S. Eggins, M. McCulloch, U-series and ESR analyses of bones and teeth relating to the human burials from Skhul. *J. Hum. Evol.* **49**, 316–334 (2005).
7. N. T. Roach, K. G. Hatala, K. R. Ostrofsky, B. Villmoare, J. S. Reeves, A. Du, D. R. Braun, J. W. K. Harris, A. K. Behrensmeyer, B. G. Richmond, Pleistocene footprints show intensive use of lake margin habitats by *Homo erectus* groups. *Sci. Rep.* **6**, 26374 (2016).
8. K. Hatala, N. T. Roach, K. R. Ostrofsky, R. E. Wunderlich, H. L. Dingwall, B. A. Villmoare, D. J. Green, J. W. K. Harris, D. R. Braun, B. G. Richmond, Footprints reveal direct evidence of group behaviour and locomotion in *Homo erectus*. *Sci. Rep.* **6**, 28766 (2016).
9. A. Cohen, M. Lockley, J. Halfpenny, A. E. Michel, Modern vertebrate track taphonomy at Lake Manyara, Tanzania. *Palaois* **6**, 371–389 (1991).
10. A. Parton, L. Clark-Balzan, A. G. Parker, G. W. Preston, W. W. Sung, P. S. Breeze, M. J. Leng, H. S. Groucutt, T. S. White, A. Alsharekh, M. D. Petraglia, Middle-late Quaternary palaeoclimate variability from lake and wetland deposits in the Nefud Desert, northern Arabia. *Quat. Sci. Rev.* **202**, 78–97 (2018).
11. T. M. Rosenberg, F. Preusser, J. Risberg, A. Plikk, K. A. Kadi, A. Matter, D. Fleitmann, Middle and late Pleistocene humid periods recorded in palaeolake deposits of the Nafud desert, Saudi Arabia. *Quat. Sci. Rev.* **70**, 109–123 (2013).
12. P. S. Breeze, H. S. Grocutt, N. A. Drake, T. S. White, R. P. Jennings, M. D. Petraglia, Palaeohydrological corridors for hominin dispersals in the Middle East ~250–70,000 years ago. *Quat. Sci. Rev.* **144**, 155–185 (2016).
13. I. Thrash, G. K. Theron, J. P. Bothma, Dry season herbivore densities around drinking troughs in the Kruger National Park. *J. Arid Environ.* **29**, 213–219 (1995).
14. M. Valeix, A. J. Loveridge, Z. Davidson, H. Madzikanda, H. Fritz, D. W. Macdonald, How key habitat features influence large terrestrial carnivore movements: Waterholes and African lions in a semi-arid savanna of north-western Zimbabwe. *Landsc. Ecol.* **25**, 337–351 (2010).
15. S. J. Armitage, S. A. Jasim, A. E. Marks, A. G. Parker, V. I. Usik, H.-P. Uerpmann, The southern route "out of Africa": Evidence for an early expansion of modern humans into Arabia. *Science* **331**, 453–456 (2011).
16. M. D. Petraglia, A. Alsharekh, P. S. Breeze, C. Clarkson, R. Crassard, N. A. Drake, H. S. Groucutt, R. Jennings, A. G. Parker, A. Parton, R. G. Roberts, C. Shipton, C. Matheson, A. al-Omari, M.-A. Veall, Hominin dispersal into the Nefud Desert and Middle Palaeolithic settlement along the Jubbah Palaeolake, northern Arabia. *PLOS ONE* **7**, e49840 (2012).
17. R. Crassard, Y. H. Hilbert, A Nubian complex site from central Arabia: Implications for Levallois taxonomy and human dispersals during the upper Pleistocene. *PLOS ONE* **8**, e69221 (2013).
18. H. S. Groucutt, T. S. White, L. Clark-Balzan, A. Parton, R. Crassard, C. Shipton, R. P. Jennings, A. G. Parker, P. S. Breeze, E. M. L. Scerri, A. Alsharekh, M. D. Petraglia, Human occupation of the Arabian Empty Quarter during MIS 5: Evidence from Mundafan Al-Buhayrah, Saudi Arabia. *Quat. Sci. Rev.* **119**, 116–135 (2015).
19. E. M. L. Scerri, P. S. Breeze, A. Parton, H. S. Groucutt, T. S. White, C. Stimpson, L. Clark-Balzan, R. Jennings, A. Alsharekh, M. D. Petraglia, Middle and late Pleistocene human habitation in the western Nefud, Saudi Arabia. *Quat. Int.* **382**, 200–214 (2015).
20. J. J. Shea, Transition or turnovers? Climatically-forced extinctions of Homo sapiens and Neanderthals in the east Mediterranean Levant. *Quat. Sci. Rev.* **27**, 2253–2270 (2008).
21. P. S. Breeze, H. S. Groucutt, N. A. Drake, J. Louys, E. M. L. Scerri, S. J. Armitage, I. S. A. Zalmout, A. M. Memesh, M. A. Haptari, S. A. Soubhi, A. H. Matari, M. Zahir, A. al-Omari, A. Alsharekh, M. D. Petraglia, Prehistory and palaeoenvironments of the western Nefud Desert, Saudi Arabia. *Arch. Res. Asia* **10**, 1–16 (2017).
22. C. R. Thouless, Long distance movements of elephants in northern Kenya. *Afr. J. Ecol.* **33**, 321–334 (1995).
23. R. M. Laws, I. S. C. Parker, R. C. B. Johnstone, *The Ecology of Elephants in North Bunyoro, Uganda* (Clarendon Press, 1975).
24. M. Ben-Dor, A. Gopher, I. Hershkovitz, R. Barkai, Man the fat hunter: The demise of *Homo erectus* and the emergence of a new hominin lineage in the middle Pleistocene (ca. 400 kyr) Levant. *PLOS ONE* **6**, e28689 (2011).
25. M. Stewart, J. L. Louys, P. S. Breeze, R. Clark-Wilson, N. A. Drake, E. M. L. Scerri, I. S. Zalmout, Y. S. A. Al-Mufarreh, S. A. Soubhi, M. A. Haptari, A. M. Alsharekh, H. S. Groucutt, M. D. Petraglia, A taxonomic and taphonomic study of Pleistocene fossil deposits from the western Nefud Desert, Saudi Arabia. *Quat. Res.* **95**, 1–22 (2020).
26. M. Stewart, J. Louys, G. J. Price, N. A. Drake, H. S. Groucutt, M. D. Petraglia, Middle and late Pleistocene mammal fossils of Arabia and surrounding regions: Implications for biogeography and hominin dispersals. *Quat. Int.* **515**, 12–29 (2019).
27. G. Haynes, On watering holes, mineral licks, death, and predation, in *Environments and Extinctions: Man in Late Glacial North America*, J. Mead, D. Meltzer, Eds. (Centre for the Study of Early Man, 1985), pp. 53–71.
28. P. Roberts, M. Stewart, A. N. Alagaili, P. S. Breeze, I. Candy, N. Drake, H. S. Groucutt, E. M. L. Scerri, J. Lee-Thorp, J. Louys, I. S. Zalmout, Y. S. A. Al-Mufarreh, J. Zech, A. Alsharekh, A. al-Omari, N. Boivin, M. D. Petraglia, Fossil herbivore stable isotopes reveal middle Pleistocene hominin palaeoenvironment in 'Green Arabia'. *Nat. Ecol. Evol.* **2**, 1871–1878 (2018).
29. G. P. Nicholas, Prehistoric hunter-gatherers in wetland environments: Theoretical issues, economic organization and resource management strategies, in *Wetland Archaeology and Environments: Regional Issues, Global Perspectives*, M. C. Lillie, S. Ellis, Eds. (Oxbow Books, 2007), pp. 46–62.
30. N. Boivin, D. Q. Fuller, R. Dennell, R. Allaby, M. D. Petraglia, Human dispersal across diverse environments of Asia during the Upper Pleistocene. *Quat. Int.* **300**, 32–47 (2013).
31. S. J. Gale, P. G. Hoare, *Quaternary Sediments: Petrographic Methods for the Study of Unlithified Rocks* (Belhaven and Halsted Press, 1991).
32. A. P. Palmer, J. A. Lee, R. A. Kemp, S. J. Carr, *Revised Laboratory Procedures for the Preparation of Thin Sections from Unconsolidated Sediments* (Centre for Micromorphology Publication, 2008).
33. S. Juggins, C2 versions 1.7.7. User guide. Software for ecological and palaeoecological data analysis and visualization (Newcastle University, 2016), p. 73.
34. R. W. Battarbee, S. Juggins, F. Gasse, N. J. Anderson, H. Bennion, N. G. Cameron, D. B. Ryves, C. Pailles, F. Chalie, R. Telford, "The European Diatom Database (EDDI): An information system for palaeoenvironmental reconstruction" (Environmental Change Research Centre Research Report No. 81, Department of Geography, University College London, 2001), p. 94.
35. F. Gasse, S. Juggins, L. B. Khelifa, Diatom-based transfer functions for inferring past hydrochemical characteristics of African lakes. *Palaeogeogr. Palaeoclimatol. Palaeoecol.* **177**, 31–54 (1995).
36. L. Bøtter-Jensen, C. E. Andersen, G. A. Duller, A. S. Murray, Developments in radiation, stimulation and observation facilities in luminescence measurements. *Radiat. Meas.* **37**, 535–541 (2003).
37. A. S. Murray, A. G. Wintle, Luminescence dating of quartz using an improved single-aliquot regenerative-dose protocol. *Radiat. Meas.* **32**, 57–73 (2000).
38. R. F. Galbraith, R. G. Roberts, J. M. Olley, H. Yoshida, G. M. Laslett, Optical dating of single and multiple grains of quartz from Jinmium Rock Shelter, Northern Australia: Part I, experimental design and statistical models. *Archaeometry* **41**, 339–364 (1999).
39. L. Bøtter-Jensen, V. Mejdahl, Assessment of beta dose-rate using a GM multicounter system. *Int. J. Radiat. Appl. Instrum. D* **14**, 187–191 (1988).

40. F. De Corte, D. Vandenberghe, S. Hossain, A. De Wispelaere, J. P. Buylaert, P. Van den Haute, Preparation and characterization of loess sediment for use as a reference material in the annual radiation dose determination for luminescence dating. *J. Radioanal. Nucl. Chem.* **272**, 311–319 (2007).
41. J. R. Prescott, J. T. Hutton, Cosmic ray and gamma ray dosimetry for TL and ESR. *Int. J. Radiat. Appl. Instrum. D* **14**, 223–227 (1988).
42. C. M. Stimpson, A. Lister, A. Parton, L. Clark-Balzan, P. S. Breeze, N. A. Drake, H. S. Groucutt, R. Jennings, E. M. L. Scerri, T. S. White, M. Zhair, M. Duval, R. Grün, A. Al-Omari, K. S. M. Al Murayyi, I. S. Zalmout, Y. A. Mufarreh, A. M. Memesh, M. D. Petraglia, Middle Pleistocene vertebrate fossils from the Nefud Desert, Saudi Arabia. *Quat. Sci. Rev.* **143**, 13–36 (2016).
43. R. Grün, Methods of dose determination using ESR spectra age estimates on tooth enamel. *Quat. Geochronol.* **4**, 231–232 (2000).
44. R. Grün, S. Brumby, The assessment of errors in past radiation doses extrapolated from ESR/TL dose-response data. *Radiat. Meas.* **23**, 307–315 (1994).
45. T. R. Clark, G. Roff, J.-x. Zhao, Y.-x. Feng, T. J. Done, J. M. Pandolfi, Testing the precision and accuracy of the U-Th chronometer for dating coral mortality events in the last 100 years. *Quat. Geochronol.* **23**, 35–45 (2014).
46. J.-x. Zhao, K.-f. Yu, Y.-x. Feng, High-precision 238U-234U-230Th disequilibrium dating of the recent past: A review. *Quat. Geochronol.* **4**, 423–433 (2009).
47. R. Grün, O. Katzenberger, An alpha irradiator for ESR dating. *Ancient TL* **12**, 35–38 (1994).
48. R. E. Marsh, "Beta-gradient isochrones using electron paramagnetic resonance: Towards a new dating method in archaeology," thesis, McMaster University, Hamilton, Ontario (1999).
49. G. Guérin, N. Mercier, G. Adamiec, Dose-rate conversion factors: Update. *Ancient TL* **29**, 5–8 (2011).
50. J. R. Prescott, J. T. Hutton, Cosmic ray contributions to dose rates for luminescence and ESR dating: Large depths and long-term time variations. *Radiat. Meas.* **23**, 497–500 (1994).
51. Q. Shao, J.-J. Bahain, J.-M. Dolo, C. Falguères, Monte Carlo approach to calculate US-ESR age and age uncertainty for tooth enamel. *Quat. Geochronol.* **22**, 99–106 (2014).
52. R. Grün, H. P. Schwarcz, J. Chadam, ESR dating of tooth enamel: Coupled correction for U-uptake and U-series disequilibrium. *Int. J. Rad. Appl. Instrum. D* **14**, 237–241 (1988).
53. Q. Shao, J.-J. Bahain, C. Falguères, J.-M. Dolo, T. Garcia, A new U-uptake model for combined ESR/U-series dating of tooth enamel. *Quat. Geochronol.* **10**, 406–411 (2012).
54. R. Grün, The DATA program for the calculation of ESR age estimates on tooth enamel. *Quat. Geochronol.* **4**, 231–232 (2009).
55. R. Grün, An alternative model for open system U-series/ESR age calculations: (Closed-system U-series)-ESR, CSUS-ESR. *Ancient TL* **18**, 1–4 (2000).
56. A. K. Behrensmeyer, Taphonomic and ecological information from bone weathering. *Paleobiology* **4**, 150–162 (1978).
57. H. T, Bunn, "Meat-eating and human evolution: Studies on the diet and subsistence patterns of Plio-Pleistocene hominids in East Africa," thesis, University of Wisconsin, Madison (1982).
58. M. R. Bennett, S. A. Morse, *Human Footprints: Fossilised Locomotion* (Springer, 2014).
59. H. L. Dingwall, K. G. Hatala, R. E. Wunderlich, B. G. Richmond, Hominin stature, body mass, and walking speed estimates based on 1.5 million-year-old fossil footprints at Ileret. *J. Hum. Evol.* **64**, 556–568 (2013).
60. M. Sponheimer, J. A. Lee-Thorp, D. de Ruiter, D. Codron, J. Codron, A. T. Baugh, F. Thackeray, Hominins, sedges, and termites: New carbon isotope data from Sterkfontein Valley and Kruger National Park. *J. Hum. Evol.* **48**, 301–312 (2005).
61. J. A. Lee-Thorp, A. Likius, H. T. Mackaya, P. Vignaud, M. Sponheimer, M. Brunet, Isotopic evidence for an early shit to C_4 resources by Pliocene hominins in Chad. *Proc. Natl. Acad. Sci. U.S.A.* **11**, 20369–20372 (2012).
62. L. E. Lisiecki, M. E. Raymo, A Plio-Pleistocene stack of 57 globally distributed benthic $\delta^{18}0$ records. *Paleoceanography* **20**, PA1003 (2005).
63. N. Mercier, H. Valladas, O. Bar-Yosef, B. Vandermeersch, C. Stringer, J.-L. Joron, Thermoluminescence date for the Mousterian burial site of Es-Skhul, Mt. Carmel. *J. Arch. Sci.* **20**, 167–174 (1993).
64. H. Valladas, J. L. Reyss, J. L. Joron, G. Valladas, O. Bar-Yosef, B. Vandermeersch, Thermoluminescence dating of Mousterian Troto-Cro-Magnon' remains from Israel and the origin of modern man. *Nature* **331**, 614–616 (1988).
65. H. S. Groucutt, E. M. L. Scerri, C. Stringer, M. D. Petraglia, Skhul lithic technology and the dispersal of *Homo sapiens* into southwest Asia. *Quat. Int.* **515**, 30–52 (2019).
66. A. Berger, M. F. Loutre, Insolation values for the climate of the last 10 million years. *Quat. Sci. Rev.* **10**, 297–317 (1991).
67. V. J. Jones, S. Juggins, The construction of a diatom-based chlorophyll *a* transfer function and its application at three lakes on Signy Island (Maritime Antarctic) subject to differing degrees of nutrient enrichment. *Freshw. Biol.* **34**, 433–445 (1995).
68. D. B. Ryves, S. Juggins, S. C. Fritz, R. W. Battarbee, Experimental diatom dissolution and the quantification of microfossil preservation in sediments. *Palaeogeogr. Palaeoclimatol. Palaeoecol.* **172**, 99–113 (2001).
69. D. B. Ryves, R. W. Battarbee, S. Juggins, S. C. Fritz, N. J. Anderson, Physical and chemical predictors of diatom dissolution in freshwater and saline lake sediments in North America and West Greenland. *Limnol. Oceanogr.* **51**, 1355–1368 (2006).
70. K. L. Loakes, D. B. Ryves, H. F. Lamb, F. Schäbitz, M. Dee, J. J. Tyler, K. Mills, S. McGowan, Late quaternary climate change in the north-eastern highlands of Ethiopia: A high resolution 15,600 year diatom and pigment record from Lake Hayk. *Quat. Sci. Rev.* **202**, 166–181 (2018).
71. R. J. Flower, Diatom preservation: Experiments and observations on dissolution and breakage in modern and fossil material. *Hydrobiologia* **269–270**, 473–484 (1993).
72. J. M. Reed, Diatom preservation in the recent sediment record of Spanish saline lakes: Implications for palaeoclimate study. *J. Paleolimnol.* **19**, 129–137 (1998).
73. J. D. Collinson, Alluvial sediments, in *Sedimentary Environments: Processes, Facies and Stratigraphy*, H. G. Reading, Ed. (Blackwell, 1996), pp. 37–81.
74. M. R. Talbot, P. A. Allen, Lakes, in *Sedimentary Environments: Processes, Facies and Stratigraphy*, H. G. Reading, Ed. (Blackwell, 1996), pp. 83–123.
75. S. J. Armitage, R. M. Bailey, The measured dependence of laboratory beta dose rates on sample grain size. *Radiat. Meas.* **39**, 123–127 (2005).
76. R. G. Roberts, R. F. Galbraith, J. M. Olley, H. Yosida, G. M. Laslett, Optical dating of single and multiple grains of quartz from Jinmium rock shelter, northern Australia: Part II, results and implications. *Archaeometry* **41**, 365–395 (1999).
77. G. A. T. Duller, Assessing the error on equivalent dose estimates derived from single aliquot regenerative dose measurements. *Ancient TL* **25**, 15–24 (2007).
78. C. Burow, calc_AliquotSize(): Estimate the amount of grains on an aliquot. Function version 1.3.2, in S. Kreutzer, M. Dietze, C. Burrow, M. C. Fuchs, C. Schmidt, M. Fischer, J. Friedrich, *Luminescence: Comprehensive Luminescence Dating Data Analysis. Rpackage Version 0.7.5* (2017); https://CRAN.R-project.org/package=Luminescence.
79. G. A. T. Duller, Distinguishing quartz and feldspar in single grain luminescence measurements. *Radiat. Meas.* **37**, 161–165 (2003).
80. A. G. Wintle, A. S. Murray, A review of quartz optically stimulated luminescence characteristics and their relevance in single-aliquot regeneration dating protocols. *Radiat. Meas.* **41**, 369–391 (2006).
81. A. G. Wintle, G. Adamiec, Optically stimulated luminescence signals from quartz: A review. *Radiat. Meas.* **98**, 10–33 (2017).
82. C. Burow, calc_CentralDose(): Apply the central age model (CAM) after Galbraith et al. (1999) to a given De distribution. Function version 1.3.2, in S. Kreutzer, M. Dietze, C. Burrow, M. C. Fuchs, C. Schmidt, M. Fischer, J. Friedrich, *Luminescence: Comprehensive Luminescence Dating Data Analysis. Rpackage Version 0.7.5* (2017); https://CRAN.R-project.org/package=Luminescence.
83. S. J. Armitage, A. Krishna, L. E. Parker, G. E. King, Optically stimulated luminescence dating of heat retainer hearths from the Sahara: Insights into signal accumulation and measurement. *Quat. Geochronol.* **45**, 249–253 (2019).
84. Y. S. Mayya, P. Morthekai, M. K. Murari, A. K. Singhvi, Towards quantifying beta microdosimetric effects in single-grain quartz dose distribution. *Radiat. Meas.* **41**, 1032–1039 (2006).
85. G. Guérin, A. S. Murray, M. Jain, K. J. Thomsen, N. Mercier, How confident are we in the chronology of the transition between Howieson's Poort and Still Bay? *J. Hum. Evol.* **64**, 314–317 (2013).
86. V. Mejdahl, Thermoluminescence dating: beta-dose attenuation in quartz grains. *Archaeometry* **21**, 61–72 (1979).
87. W. T. Bell, Attenuation factors for the absorbed radiation dose in quartz inclusions for thermoluminescence dating. *Ancient TL* **8**, 12 (1979).
88. G. A. T. Duller, The age of the Koputaroa dunes, southwest North Island, New Zealand. *Palaeogeogr. Palaeoclimatol. Palaeoecol.* **121**, 105–114 (1996).
89. J. A. Durcan, G. E. King, G. A. T. Duller, DRAC: Dose Rate and Age Calculator for trapped charge dating. *Quat. Geochronol.* **28**, 54–61 (2015).
90. M. Dietze, S. Kreutzer. Plot_AbanicoPlot(): Function to create an Abanico Plot. Function version 1.3.2, in S. Kreutzer, M. Dietze, C. Burrow, M. C. Fuchs, C. Schmidt, M. Fischer, J. Friedrich, *Luminescence: Comprehensive Luminescence Dating Data Analysis. Rpackage Version 0.7.5* (2017); https://CRAN.R-project.org/package=Luminescence.
91. M. Dietze, S. Kreutzer, C. Burow, M. C. Fuchs, M. Fischer, C. Schmidt, The abanico plot: Visualising chronometric data with individual standard errors. *Quat. Geochronol.* **31**, 12–18 (2016).
92. M. Duval, R. Grün, Are published ESR dose assessments on fossil tooth enamel reliable? *Quat. Geochronol.* **31**, 19–27 (2016).
93. A. W. G. Pike, R. E. M. Hedges, Sample geometry and U uptake in archaeological teeth: Implication for U-series and ESR dating. *Quat. Sci. Rev.* **20**, 2012–2025 (2001).
94. M. Sambridge, R. Grün, S. Eggins, U-series dating of bone in an open system: The diffusion-adsorption-decay model. *Quat. Geochronol.* **9**, 42–53 (2012).

95. M. Duval, C. Falguères, J. -J. Bahain, Age of the oldest hominin settlements in Spain: Contribution to the combined U-series/ESR dating method applied to fossil teeth. *Quat. Geocrhonol.* **10**, 412–417 (2012).
96. J.-J. Bahain, Y. Yokoyama, C. Falguères, M. N. Sarcia, ESR dating of tooth enamel: A comparison with K-Ar dating. *Quat. Sci. Rev.* **11**, 245–250 (1992).
97. W. J. Rink, H. P. Schwarcz, H. K. Lee, J. Rees-Jones, R. Rabinovich, E. Hovers, Electron spin resonance (ESR) and thermal ionization mass spectrometric (TIMS) 230Th/234U dating of teeth in Middle Paleolithic layers at Amud Cave, Israel. *Geoarchaeology* **16**, 701–717 (2001).
98. M. Duval, L. Martin, An application of DosiVox to ESR dating of fossil teeth: Evaluating the impact of dental tissue thickness on the external beta dose rate evaluation. *Geochronometria* **46**, 102–110 (2019).
99. H. Cheng, R. L. Edwards, J. Hoff, C. D. Gallup, D. A. Richards, Y. Asmerom, The half-lives of uranium-234 and thorium-230. *Chem. Geol.* **169**, 17–33 (2000).
100. M. Stewart, J. Louys, H. S. Groucutt, I. Candy, R. Clark-Wilson, P. S. Breeze, N. A. Drake, G. J. Price, Y. S. A. Al-Mufarreh, S. A. Soubhi, I. S. Zalmout, A. M. Alsharekh, A. al-Omari, M. D. Petraglia, Taphonomic and zooarchaeological investigations at the middle Pleistocene site of Ti's al Ghadah, western Nefud Desert, Saudi Arabia. *Quat. Sci. Rev.* **218**, 228–253 (2019).
101. H. A. McClure, "Late Quaternary palaeoenvironments of the Rub' al Khali", thesis, University College, London (1984).
102. N. Ashton, S. G. Lewis, I. De Groote, S. M. Duffy, M. Bates, R. Bates, P. Hoare, M. Lewis, S. A. Parfitt, S. Peglar, C. Williams, C. Stringer, Hominin footprints from early Pleistocene deposits at Happisburgh, UK. *PLOS ONE* **9**, e88329 (2014).
103. A. L. A. Wiseman, I. De Groote, A three-dimensional geometric morphometric study of the effects of erosion on the morphologies of modern and prehistoric footprints. *J. Archaeol. Sci. Rep.* **17**, 93–102 (2018).
104. B. Zimmer, G. Pierce-Liutkus, S. T. Marshall, K. G. Hatala, A. Metallo, V. Rossi, Using differential structure-from-motion photogrammetry to quantify erosion at the Engare Sero footprint site, Tanzania. *Quat. Sci. Rev.* **198**, 226–241 (2018).
105. J. Duveau, G. Berillon, C. Verna, G. Laisne, D. Cliquet, The composition of a Neanderthal social group revealed by the hominin footprints at Le Rozel (Normandy, France). *Proc. Natl. Acad. Sci. U.S.A.* **116**, 19409–19414 (2019).
106. M. D. Leakey, R. L. Hay, Pliocene footprints in the Laetoli Beds at Laetoli, northern Tanzania. *Nature* **278**, 317–323 (1979).
107. M. H. Day, E. H. Wickens, Laetoli Pliocene hominid footprints and bipedalism. *Nature* **286**, 385–387 (1980).
108. D. A. Raichlen, A. D. Gordon, W. E. Harcourt-Smith, A. D. Foster, W. R. Haas Jr., Laetoli footprints preserve earliest evidence of human-like bipedal biomechanics. *PLOS ONE* **5**, e9769 (2010).
109. R. H. Crompton, T. C. Pataky, R. Savage, K. D'Août, M. R. Bennett, M. H. Day, K. Bates, S. Morse, W. I. Sellers, Human-like external function of the foot, and fully upright gait, confirmed in the 3.66 million year old Laetoli hominin footprints by topographic statistics, experimental footprint-formation and computer simulations. *J. Royal Soc. Interface* **9**, 707–719 (2011).
110. K. G. Hatala, N. T. Roach, K. R. Ostrofsky, R. E. Wunderlich, H. L. Dingwall, B. A. Villmoare, D. J. Green, D. R. Braun, J. W. K. Harris, A. K. Behrensmeyer, B. G. Richmond, Hominin track assemblages from Okote Member deposits near Ileret, Kenya, and their implications for understanding fossil hominin paleobiology at 1.5 Ma. *J. Hum. Evol.* **112**, 93–104 (2017).
111. M. R. Bennett, J. W. K. Harris, B. G. Richmond, D. R. Braun, E. Mbua, P. Kiura, D. Olago, M. Kibunjia, C. Omuombo, A. K. Behrensmeyer, D. Huddart, S. Gonzalez, Early hominin foot morphology based on 1.5-million-year-old footprints from Ileret, Kenya. *Science* **323**, 1197–1201 (2009).
112. N. T. Roach, A. Du, K. Hatala, K. R. Ostrofsky, J. S. Reeves, D. R. Braun, J. W. K. Harris, A. K. Behrensmeyer, B. G. Richmond, Pleistocene animal communities of a 1.5 million-year-old lake margin grassland and their relationship to *Homo erectus* paleoecology. *J. Hum. Evol.* **122**, 70–83 (2018).
113. F. Altamura, M. R. Bennett, K. D'Août, S. Gaudzinski-Windheuser, R. T. Melis, S. C. Reynolds, M. Mussi, Archaeology and ichnology at Gombore II-2, Melka Kunture, Ethiopia: Everyday life of a mixed-age hominin group 700,000 years ago. *Sci. Rep.* **8**, 2815 (2018).
114. S. Webb, M. L. Cupper, R. Robins, Pleistocene human footprints from the Willandra Lakes, southeastern Australia. *J. Hum. Evol.* **50**, 405–413 (2006).
115. D. Bustos, J. Jakeway, T. M. Urban, V. T. Holliday, B. Fenerty, D. A. Raichlen, M. Budka, S. C. Reynolds, B. D. Allen, D. W. Love, V. L. Santucci, D. Odess, P. Willey, H. G. McDonald, M. R. Bennett, Footprints preserve terminal Pleistocene hunt? Human-sloth interactions in North America. *Sci. Adv.* **4**, eaar7621 (2018).
116. N. Panin, E. Avram, Noi urme de vertebrate in Miocenul Subcarpatilor Rominesti (Nouvelles empreintes de vertèbres dans le Miocène de la zone subcarpathique roumaine). *Studii si Cercetari de Geologie* **7**, 455–484 (1962).
117. C. Neto de Carvalho, S. Figueiredo, J. Belo, Vertebrate tracks and trackways from the Pleistocene eolianites of SW Portugal. *Comunicaçõe Geológicas* **103**, 101–116 (2016).
118. P. McNeil, L. V. Hills, M. S. Tolman, B. Kooyman, Significance of latest Pleistocene tracks, trackways, and trample grounds from souther Alberta, Canada, in *Cenozoic Vertebrate Tracks*, S. G. Lucas, J. A. Spielmann, M. G. Lockely, Eds. (New Mexico Museum of Natural History, 2007), pp. 209–224.
119. C. Neto de Carvalho, Vertebrate tracksites from the mid-late Pleistocene eolianites of Portugal: The first record of elephant tracks in Europe. *Geol. Q.* **53**, 407–414 (2009).
120. M. P. Pasenko, Quantitative and qualitative data of footprints produced by Asian (*Elephas maximus*) and African (*Loxodonta africana*) elephants and with a discussion of significance towards fossilized proboscidean footprints. *Quat. Int.* **433**, 221–227 (2017).
121. D. Western, C. Moss, N. Georgiadis, Age estimation and population age structure of elephants from footprint dimensions. *J. Wildl. Manag.* **47**, 1192–1197 (1983).
122. W. J. Sanders, E. Gheerbrant, J. M. Harris, H. Saegusa, C. Delmer, Proboscidea, in *Cenozoic Mammals of Africa*, L. Werdelin, W. J. Sanders. Eds. (Univerity of California Press, 2010), pp. 161–252.
123. Y. Coppens, V. J. Maglio, C. T. Madden, M. Beden, Proboscidea, in *Evolution of African Mammals*, V. J. Maglio, H. B. S. Cooke, Eds. (Harvard University Press, 1978), pp. 336–367.
124. A. J. Stuart, The extinction of woolly mammoth (*Mammuthus primigenius*) and straight-tusked elephant (*Palaeoloxodon antiquus*) in Europe. *Quat. Int.* **126–128**, 171–177 (2005).
125. D. Pushkina, The Pleistocene easternmost distribution in Eurasia of the species associated with the Eemian *Palaeoloxodon antiquus* assemblage. *Mammal Rev.* **37**, 224–245 (2007).
126. N. Porat, Luminensence and electron spin resonance dating, in *Holon, a Lower Paleolithic Site in Israel*, M. Chazan, L. Kolska-Horwitz, Eds. (Peabody Museum of Archaeology and Ethnology, Harvard Univ., 2007), pp. 27–42.
127. O. Bar-Yosef, M. Belmaker, Early and middle Pleistocene faunal and hominin dispersals through southwestern Asia. *Quat. Sci. Rev.* **30**, 1318–1337 (2011).
128. J. T. Pokines, A. M. Lister, C. J. H. Ames, A. Nowell, C. E. Cordova, Faunal remains from recent excavations at Shishan Marsh 1 (SM1), a late Lower Palaeolithic open-air site in the Azraq Basin, Jordan. *Quat. Res.* **91**, 768–791 (2019).
129. A. M. Lister, W. Dirks, A. Assaf, M. Chazan, P. Goldberg, Y. H. Applbaum, N. Greenbaun, L. K. Horwitz, New fossil remains of *Elephas* from the southern levant: Implications for the evolutionary history of the Asian elephant. *Palaeogeogr. Palaeoclimatol. Palaeoecol.* **386**, 119–130 (2013).
130. A. Delagnes, C. Tribolo, P. Bertran, M. Brenet, R. Crassard, J. Jaubert, L. Khalidi, N. Mercier, S. Nomade, S. Peigné, L. Sitzia, J. F. Tournepiche, M. Al-Halibi, A. Al-Mosabi, R. MacChiarelli, Inland human settlement in southern Arabia 55,000 years ago. New Evidence from the Wadi Surdud Middle Palaeolithic site complex, western Yemen. *J. Hum. Evol.* **63**, 452–474 (2012).
131. C. Stuart, *Field Guide to Tracks and Signs of Souther, Central, and East African Wildlife* (Penguin Random House, 2013).
132. L. Liebenberg, *Photographic Guide to Tracks and Tracking in Southern Africa* (Penguin Random House, 2014).
133. H. Thomas, D. Geraads, D. Janjou, D. Vaslet, A. Memesh, D. Billiou, H. Bocherens, G. Dobigny, V. Eisenmann, M. Gayet, F. Lapparent de Broin, G. Petter, M. Halawani, First Pleistocene faunas from the Arabian peninsula: An Nafud desert, Saudi Arabia. *C. R. Acad. Sci.* **326**, 145–152 (1998).
134. M. Guagnin, C. Shipton, S. el-Dossary, M. al-Rashid, F. Moussa, M. Stewart, F. Ott, A. Alsharekh, M. D. Petraglia, Rock art provides new evidence on the biogeography of kudu (*Tragelaphus imberbis*), wild dromedary, aurochs (*Bos primigenius*) and African wild ass (*Equus africanus*) in the early and middle Holocene of north-western Africa. *J. Biogeogr.* **45**, 727–740 (2018).
135. S. G. Lucas, A. P. Hunt, Ichnotaxonomy of camel footprints, in *Cenozoic Vertebrate Tracks*, S. G. Lucas, J. A. Spielmann, M. G. Lockely, Eds. (New Mexico Museum of Natural History, 2007), pp. 155–168.
136. D. J. Meldrum, M. G. Lockley, P. G. Lukas, C. Musiba, Ichnotaxonomy of the Laetoli trackways: The earliest hominin footprints. *J. Afr. Earth Sci.* **60**, 1–12 (2011).
137. J. Y. Kim, K. S. Kim, M. G. Lockley, N. Matthews, Hominid ichnotaxonomy: An exploration of a neglected discipline. *Ichnos* **15**, 126–139 (2008).
138. R. Crassard, M. D. Petraglia, N. A. Drake, P. Breeze, B. Gratuze, A. Alsharekh, M. Arbach, H. S. Groucutt, L. Khalidi, N. Michelsen, C. J. Robin, J. Schiettecatte, Middle Palaeolithic and Neolithic occupations around Mundafan Palaeolake, Saudi Arabia: Implications for climate change and human dispersals. *PLOS ONE* **8**, e9665 (2013).
139. D. A. E. Garrod, D. M. A. Bate, *The Stone Age of Mount Carmel* (Clarendon Press, 1937).
140. O. Bar-Yosef, J. Callander, The woman from Tabun: Garrod's doubts in historical perspective. *J. Hum. Evol.* **37**, 879–885 (1999).
141. R. Grün, C. Stringer, Tabun revisited: Revised ESR chronology and new ESR and U-series analyses of dental material from Tabun C1. *J. Hum. Evol.* **36**, 601–612 (2000).

142. N. Mercier, H. Vallasas, Reassessment of the TL age estimates of burnt flints from the Paleolithic site of Tabun Cave, Israel. *J. Hum. Evol.* **45**, 401–409 (2003).
143. K. Harvati, E. N. Lopez, A 3-D look at the Tabun C2 jaw, in *Human Paleontology and Prehistory*, A. Marom, E. Hovers, Eds. (Springer, 2017), pp. 203–213.
144. Y. Shu, Q. Mei, J. Fernandez, Z. Li, N. Feng, Y. Gu, Foot morphological difference between habitually shod and unshod runnerts. *PLOS ONE* **10**, e0131385 (2015).
145. S. A. Morse, M. R. Bennett, C. Liutkus, F. Thackeray, J. McClymont, R. Savage, R. H. Crompton, Holocene footprints in Namibia: The influence of substrate on footprint morphology. *Am. J. Phys. Anthropol.* **151**, 265–279 (2013).
146. S. Webb, Further research of the Willandra Lakes fossil footprint site, southeastern Australia. *J. Hum. Evol.* **52**, 711–715 (2007).
147. M. Avanzini, P. Mietto, A. Panarello, M. D. Angelis, G. Rolandi, The Devil's Trails: Middle Pleistocene human footprints preserved in a volcanoclastic deposit of southern Italy. *Ichnos* **15**, 179–189 (2008).
148. M. Will, A. Pablos, J. T. Stock, Long-term patterns of body mass and stature evolution within the hominin lineage. *R. Soc. Open Sci.* **4**, 171339 (2017).
149. M. R. Feldesman, J. G. Kleckner, J. K. Lundy, Femur/stature ratio and estimates of stature in mid- and late-Pleistocene fossil hominids. *Yearb. Phys. Anthropol.* **83**, 359–372 (1990).
150. J.-M. Carretero, L. Rodríguez, R. García-Conzález, J.-L. Arsuaga, A. Gómez-Olivencia, C. Lorenzo, A. Bonmatí, A. Gracia, I. Martínez, R. Quam, Stature estimation from complete long bones in the middle Pleistocene humans from the Sima de los Huesos, Sierra de Atapuerca (Spain). *J. Hum. Evol.* **62**, 242–255 (2012).
151. C. B. Ruff, M. L. Burgess, N. Squyres, J.-A. Junno, E. Trinkaus, Lower limb articular scaling and body mass estimations in Pliocene and Pleistocene hominins. *J. Hum. Evol.* **115**, 85–111 (2018).
152. A. Rohatgi, Web Plot Digitizer, Verson 4.1 (2018); https://automeris.io/WebPlotDigitizer/.
153. R. P. Jennings, J. Singarayer, E. J. Stone, U. Krebs-Kanzow, V. Khon, K. H. Nisancioglu, M. Pfeiffer, X. Zhang, A. Parker, A. Parton, H. S. Groucutt, T. S. White, N. A. Drake, M. D. Petraglia, The greening of Arabia: Multiple opportunities for human occupation of the Arabian Peninsula during the late Pleistocene inferred from an ensemble of climate model simulations. *Quat. Int.* **382**, 181–191 (2015).
154. D. Fleitmann, S. J. Burns, U. Neff, A. Mangini, A. Matter, Changing moisture sources over the last 330,000 years in northern Oman from fluid-inclusion evidence in speleothems. *Quat. Res.* **60**, 223–232 (2003).
155. D. Fleitmann, S. J. Burns, M. Pekala, A. Mangini, A. Al-Subbary, M. Al-Aowah, J. Kramer, A. Matter, Holocene and Pleistocene pluvial periods in Yemen, southern Arabia. *Quat. Sci. Rev.* **30**, 783–787 (2011).
156. J. A. Lee-Thorp, J. C. Sealy, N. J. van der Merwe, Stable carbon isotope ratio differences between collagen and bone apatite, and their relationship to diet. *J. Archaeol. Sci.* **16**, 585–599 (1989).
157. J. A. Lee-Thorp, N. J. van der Merwe, C. K. Brain, Isotopic evidence for dietary differences between two extinct baboon species from Swartkrans (South Africa). *J. Hum. Evol.* **18**, 183–190 (1989).
158. N. E. Levin, S. W. Simpson, J. Quade, T. E. Cerling, S. R. Frost, Herbivore enamel carbon isotopic composition and the environmental context of *Ardipithecus* at Gona, Ethiopia, in *The Geology of Early Humans in the Horn of Africa*, J. Quade, J. G. Wynn, Eds. (Geological Society of America Special Paper, 2008), pp. 2015–234.
159. M. Calvin, A. A. Benson, The path of carbon in photosynthesis. *Science* **107**, 476–480 (1948).
160. M. D. Hatch, C. R. Slack, H. S. Johnson, Further studies on a new pathway of photosynthetic carbon dioxide fixation in sugarcane and its occurrence in other plant species. *Biochem. J.* **102**, 417–422 (1967).
161. L. Tieszen, Natural variations in the carbon isotope values of plants: Implications for archaeology, ecology, and paleoecology. *J. Archaeol. Sci.* **18**, 227–248 (1991).
162. W. Dansgaard, Stable isotopes in precipitation. *Tellus* **16**, 436–468 (1964).
163. N. Buchmann, J. R. Ehleringer, CO_2 concentration profiles, and carbon and oxygen isotopes in C_3 and C_4 crop canopies. *Agric. For. Meteorol.* **89**, 45–58 (1998).
164. M. Sponheimer, J. A. Lee-Thorp, The oxygen isotope composition of mammalian enamel carbonate from Morea Estate, South Africa. *Oecologia* **126**, 153–157 (2001).
165. M. J. Kohn, M. J. Schoeninger, J. W. Valley, Herbivore tooth oxygen isotope compositions: Effects of diet and physiology. *Geochim. Cosmochim. Acta* **60**, 3889–3896 (1996).
166. N. E. Levin, T. E. Cerling, B. H. Passey, J. M. Harris, J. R. A. Ehleringer, Stable isotope aridity index for terrestrial environments. *Proc. Natl. Acad. Sci. U.S.A.* **103**, 11201–11205 (2006).
167. S. A. Blumenthal, L. E. Levin, F. H. Brown, J. -P. Brugal, K. L. Chritz, J. M. Harris, G. E. Jehle, T. E. Cerling, Aridity and hominin environments. *Proc. Natl. Acad. Sci. U.S.A.* **114**, 7331–7336 (2017).
168. L. B. Flanagan, J. P. Comstock, J. R. Ehleringer, Comparison of modelled and observed environmental influences on the stable oxygen and hydrogen isotope composition of leaf water in *Phaseolus vulgaris L. Plant Physiol.* **96**, 588–596 (1991).
169. M. M. Barbour, Stable oxygen isotope composition of plant tissue: A review. *Funct. Plant Biol.* **34**, 83–94 (2007).
170. Y. Wang, T. E. Cerling, A model of fossil tooth and bone diagensis: Implications for paleodiet reconstruction from stable isotopes. *Palaeogeogr. Palaeoclimatol. Palaeoecol.* **107**, 271–289 (1994).
171. J. A. Lee-Thorp, Preservation of biogenic carbon isotopic signals in Plio-Pleistocene bone and tooth mineral, in *Biogeochemical Approaches to Paleodietary Analysis*, S. H. Ambrose, M. A. Katzenberg, Eds. (Kluwer Academic/Plenum Publishers, 2000), pp. 89–115.
172. S. H. Ambrose, L. Norr, Experimental evidence for the relationship of the carbon isotope ratios of whole diet and dietary protein to those of bone collagen and carbonate, in *Prehistoric Human Bone: Archaeology at the Molecular Leval*, J. B. Lambert, G. Grupe, Eds. (Springer, 1993), pp. 1–37.
173. M. Balasse, Reconstructing dietary and environmental history from enamel isotopic analysis. Time resolution of intra-tooth sequential sampling. *Int. J. Osteoarchaeol.* **12**, 115–165 (2002).
174. M. O'Leary, Carbon isotope fractionation in plants. *Phytochemistry* **20**, 553–567 (1981).
175. K. R. Ludwig, A geochronological toolkit for Microsoft Excel (Special Publication, No. 5, Berkely Geochronological Centre, 2012).

Acknowledgments: We would like to thank the Saudi Commision for Tourism and National Heritage (SCTH) for continued support of the Palaeodeserts Project. **Funding:** The Palaeodeserts Project is supported by the Max Planck Society, European Research Council (no. 295719 to M.D.P.), Bristish Academy, and Leverhulme trust (PG-2017-087). M.S. would like to thank the Leakey Foundation for generous funding. R.C.-W.'s contribution to this work was supported by a Natural Environmental Research Council DRP studentship, and data relating to this contribution can be found in the texts S1 and S2. P.S.B.'s research is supported by the Leverhulme Trust (ECF-2019-538). M.D.'s research is supported by the Australian Research Council (ARC) Future Fellowship grant (FT150100215). S.J.A.'s contribution to this work was partly supported by the Research Council of Norway, through its Centres of Excellence funding scheme, SFF Centre for Early Sapiens Behaviour (SapienCE) (no. 262618). J.L.'s research is supported by the Australia Research Council (ARC) Future Fellowship Grant (FT160100450). A.M.A. acknowledges the financial support of the Researchers Supporting Project Number (RSP-2019/126), King Saud University, Riyadh, Saudi Arabia. **Author contributions:** M.S., R.C.-W., P.S.B., K.J., I.C., S.J.A., J.L., G.J.P., P.C., M.A.B., N.A.D., H.S.G., A.M.A., B.Z., A.A.-O., and M.D.P. conceived the project. M.S. performed the analysis of fossil material. R.C.-W., S.J.A., and I.C. conducted the sediment and OSL dating analyses. P.S.B. coordinated on-site surveys and produced site maps. G.J.P. and M.D. performed the uranium-series and ESR dating study. D.B.R. performed the diatom analysis. P.R. performed the stable isotope analysis. M.S. and R.C.-W wrote the manuscript with support from J.L., M.D., G.J.P., D.B.R., I.C., S.J.A., P.R., and H.S.G. All authors contributed to the manuscript and approved the final version, and all authors qualifying for authorship are listed. **Competing interests:** The authors declare that they have no competing interests. **Data and materials availability:** All data needed to evaluate the conclusions in the paper are present in the paper and/or Supplementary Materials. Additional data may be requested from the authors.

Submitted 14 January 2020
Accepted 31 July 2020
Published 18 September 2020
10.1126/sciadv.aba8940

Citation: M. Stewart, R. Clark-Wilson, P. S. Breeze, K. Janulis, I. Candy, S. J. Armitage, D. B. Ryves, J. Louys, M. Duval, G. J. Price, P. Cuthbertson, M. A. Bernal, N. A. Drake, A. M. Alsharekh, B. Zahrani, A. Al-Omari, P. Roberts, H. S. Groucutt, M. D. Petraglia, Human footprints provide snapshot of last interglacial ecology in the Arabian interior. *Sci. Adv.* **6**, eaba8940 (2020).

Human footprints provide snapshot of last interglacial ecology in the Arabian interior

Mathew Stewart, Richard Clark-Wilson, Paul S. Breeze, Klint Janulis, Ian Candy, Simon J. Armitage, David B. Ryves, Julien Louys, Mathieu Duval, Gilbert J. Price, Patrick Cuthbertson, Marco A. Bernal, Nick A. Drake, Abdullah M. Alsharekh, Badr Zahrani, Abdulaziz Al-Omari, Patrick Roberts, Huw S. Groucutt and Michael D. Petraglia

Sci Adv **6** (38), eaba8940.
DOI: 10.1126/sciadv.aba8940